CHAPTER III

MATERIALS AND METHODS

This chapter describes the preparation, various characterization techniques that were employed to examine the structural, optical, morphological, magnetic and electrochemical impedance analysis of undoped and doped CuI nanoparticles and thin films.

3.1 Reagents

- ✓ The chemicals employed in our research work viz., sodium thiosulfate (HIMEDIA) and potassium iodide (HIMEDIA) were purchased in pure form and used as such.

- ✓ The metal salts used are copper (II) chloride dihydrate ($CuCl_2.2H_2O$) (MERCK), copper (II) sulphate pentahydrate ($CuSO_4.5H_2O$) (MERCK), manganese (II) chloride hexahydrate ($MnCl_2.4H_2O$) (Merck).

- ✓ Deionised water was used throughout the experiments.

3.2 Preparation of the nanoparticles and thin films

3.2.1 Preparation of CuI nanoparticles

In a typical synthesis, 100 mL of 0.5 M reducing agent sodium thiosulphate solution was added in drops to 100 mL of 0.5 M aqueous solution of copper (II) chloride dehydrate solution with constant stirring. To the stirred solution, aqueous solution of potassium iodide is added drop by drop and a brown colour precipitate is formed, which was filtered, washed and dried in oven at 60°C for 4 hours.

3.2.2 Preparation of CuI thin films

The thin films of CuI were deposited in accordance with SILAR method (R. N. Bulakhe et.al, 2013) on prepared glass substrates. The glass surfaces were modified by employing wet and dry chemical cleaning methods prior to the deposition of thin films so as

to improve the adhesive bonding between the glass surface and thin films. Substrates were washed with methanol and deionised water successively and dried at 120°C. The substrates were first immersed in a solution containing 0.1 M $CuSO_4.5H_2O$, which was used as the cationic percursor and 0.1 M $Na_2S_2O_3$ for 40 seconds. $Na_2S_2O_3$ play the role of both reducing and complexing agent and reduces Cu^{2+} to Cu^+. Finally the substrates were immersed in a solution of 0.025 M KI for another 40 seconds. The substrates were then rinsed with deionised water to remove the loosely held ions and dried the substrates at 60°C for 4 hours and stored air tight.

3.2.3 Preparation of Manganese doped copper iodide thin films

The manganese doped CuI thin films with two different concentrations of manganese were deposited on the glass substrates. $CuSO_4.5H_2O$ and $MnCl_2$. $4H_2O$ were dissolved in 50 mL of deionised water. The concentration for $CuSO_4.5H_2O$ was 0.2 M and the concentrations of $MnCl_2.4H_2O$ were 0.01 M (5 mol% doping) and 0.02 M (10 mol% doping) respectively. The resultant mixtures were then subjected to stirring at room temperature for 1 h to obtain homogeneity. The glass substrates were cleaned with methanol for 15 minutes rinsed using deionized water and then dried in hot air oven prior to the deposition of the films. The CuI films and Mn doped CuI thin films were prepared without and with including $MnCl_2.4H_2O$ in the above mentioned procedure. The doped thin films were then dried for a period of 2 hours at 60°C in a hot air oven.

3.2.4 Preparation of Magnesium doped copper iodide nanoparticles

The Mg doped CuI nanoparticles was prepared by conventional precipitation method. About 50 mL of 0.5 M reducing agent sodium thiosulphate solution was added in drops to the solutions containing 50 mL of 0.5 M aqueous solution of copper (II) chloride dehydrate solution and 0.01 M(5 mol%) and 0.02 M(10 mol%) aqueous solution of magnesium (II) chloride hexahydrate with constant stirring. To the stirred solution, aqueous solution of

potassium iodide is added drop by drop and a brown colour precipitate is formed, which was filtered, washed and dried in oven at 60°C for 4 hours.

3.3 Characterisation techniques

3.3.1 X-ray diffraction studies (XRD)

The crystal structure of the synthesized samples is analyzed using PANalyticalX'Pert PRO powder X-ray Diffractometer, at a scanning range angle of 10–100°with CuKα radiation of wavelength of k =1.5406 Å. The XRD analyzes the crystalline states under normal atmospheric conditions. This method is non destructive. X-rays focused on a sample fixed on the axis of the spectrometer (goniometer) are diffracted by the sample. The changes in the diffracted X-ray intensities are measured, recorded and plotted against the rotation angles of the sample. The result is referred to as the XRD pattern of the sample.

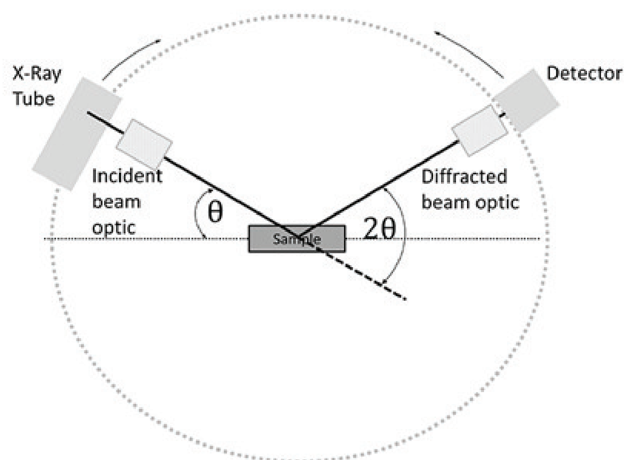

Fig 3.1 Experimental set-up of X-ray diffractometer

Computer analysis of the peak positions and intensities associated with this pattern enables qualitative analysis, lattice constant determination and / or stress determination of the sample. Qualitative analysis may be conducted on the basis of peak height or peak area. The peak angles and profiles may be used to determine particle diameters and degree of crystallization and are useful in conducting precise X-ray structural analysis. The intensity of the reflected beam at certain angles will be maximum when the path difference between

two reflected waves from two different planes is an integral multiple of λ. This condition is called Bragg's law (W.L. Bragg, 1912)and is given by the relation,

$$2d\sin\theta = n\lambda$$

Where n is the order of diffraction, λ is the wavelength of the X-rays, d is the spacing between consecutive parallel planes and $\theta$is the glancing angle (or the complement of the angle of incidence) (C. Kittel, 1996). Every Crystalline substance gives a pattern; the same substance always gives the same pattern; and in a mixture of substances each produces its pattern independently of the others. X-ray diffraction studies give a whole range of informationabout the crystal structure, orientation, average crystallite size and stress in the samples. Experimentally obtained diffraction patterns of the sample are compared with the standard powder diffraction files published by the International Centre for Diffraction Data (ICDD), formerly JCPDS (Joint Committee on Powder Diffraction Standards).

3.3.2 Fourier Transform Infrared Spectroscopy (FTIR)

The FTIR spectra for the samples were recorded using Perkin Elmer spectrometer in the wavenumber range of 400-4000 cm^{-1}.Infrared spectroscopy is the method of choice of qualitative analysis of organic material and it has wide application to inorganic substances as well. Molecular vibrations in the sample can be detected by the vibration spectroscopy. It is well known that, IR encompasses a spectral region from red end of visible spectrum (12,500cm^{-1}, 0.8 mm) to the microwave 10 cm^{-1}, 1000 mm) in the electromagnetic spectrum. When exposed to infrared radiation, sample molecules selectively absorb radiation of specific wavelengths which causes the change of dipole moment of sample molecules. Consequently, the vibrational energy levels of sample molecules transfer from ground state to excited state. The frequency of the absorption peak is determined by the vibrational energy gap. The number of absorption peaks is related to the number of vibrational freedom of the molecule. The intensity of absorption peaks is related to the change of dipole moment and the

possibility of the transition of energy levels. Therefore, by analyzing the infrared spectrum, one can readily obtain abundant structure information of a molecule.

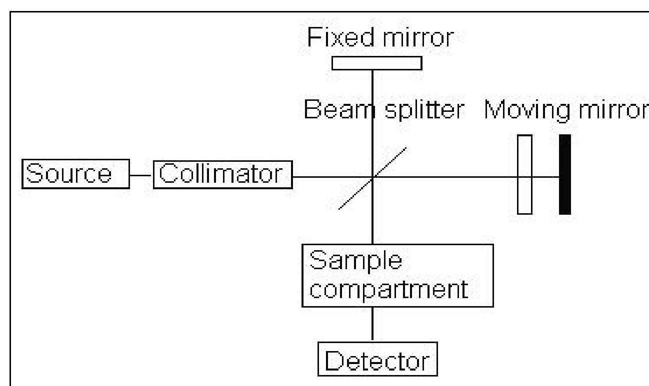

Fig 3.2 Block diagram of an FTIR spectrometer

However, based upon applications and instrumentation involved, it is divided in to near-IR (12,500 to 4000 cm^{-1}), mid-IR (4000 to 400 cm^{-1}) and far-IR (400 to 10 cm^{-1}). It is found that most of the fundamental molecular vibrations occur in mid-IR region. FTIR spectrometers are based upon Michelson interferometer. A typical spectrometer mainly consists of components like (a) radiation source, which is always Nernst filament (ZrO_2 + Y_2O_3) or Globar (SiC), (b) optical path and monochromator, in which the beam is guided and focused by the mirrors aluminized or silverized on their surfaces, (c) detectors for heat radiations detecting.The source generates radiation which passes the sample through the interferometer and reaches the detector. Then the signal is amplified and converted to digital signal by the amplifier and analog-to-digital converter, respectively. Eventually, the signal is transferred to a computer in which Fourier transform is carried out.

3.3.3 Scanning electron micrographs (SEM)

The SEM images were acquired using JEOL JSM-6390 electron microscope at the accelerating voltage of 20kV. A scanning electron microscope (SEM) scans a focused electron beam over a surface to create an image. The electrons in the beam interact with the sample, producing various signals that can be used to obtain information about the surface

topography and composition. SEMs use an electron beam instead of a beam of light, which is directed towards the specimen under examination. An electron gun, located at the top of the device, shoots out a beam of highly concentrated electrons. There are two main types of electron guns used by SEMs.The first, Thermionic guns, heat a filament until electrons stream away. Field emission guns, the other popular choice, rip electrons away from their atoms by generating a strong electrical field.

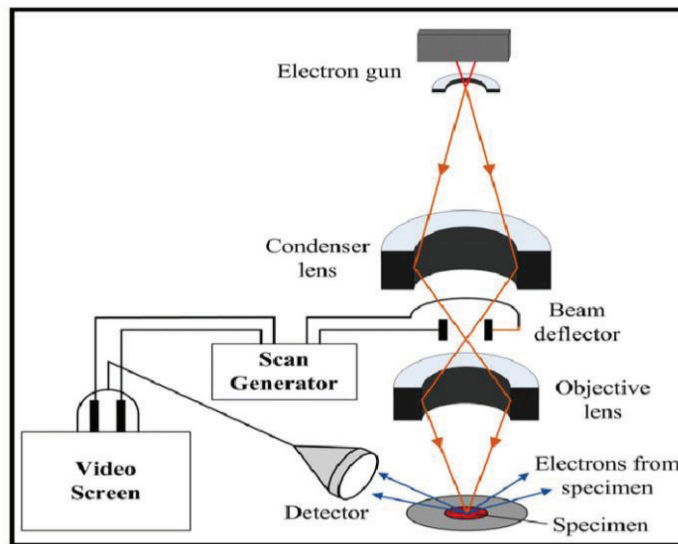

Fig 3.3 Schematic diagram of SEM

The microscope is composed of a series of lenses within a vacuum chamber. These lenses direct the electrons towards the specimen in order to maximize efficiency. The SEM usually requires a vacuum chamber to function, as the electron beam must not be obstructed as it passes through the body of the microscope. Small particles could deflect the electrons onto the specimen itself, obscuring the results.

When a specimen is hit with a beam of the electrons known as the incident beam, it emits X-rays and three kinds of electrons: primary backscattered electrons, secondary electrons and Auger electrons. The SEM uses primary backscatter electrons and secondary electrons.An electron recorder picks up the rebounding electrons and records their imprint.

This information is translated onto a screen which allows three-dimensional images to be represented clearly.

3.3.4 Energy dispersive X-ray analysis (EDAX)

EDAX is an analytical technique used for elemental analysis or chemical characterization of a sample. It is based on the investigation of a sample through interactions between electromagnetic radiation and matter, analyzing X-rays emitted by the matter in response to being hit with the electromagnetic radiation. Its characterization capabilities are due in large part to the fundamental principle that each element has a unique atomic structure allowing X-rays that are characteristic of an element's atomic structure to be identified uniquely from each other.

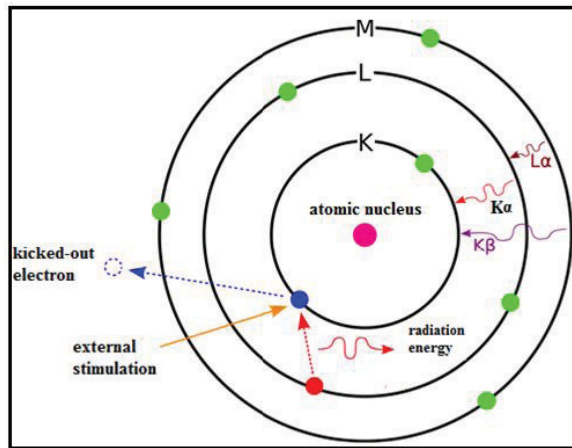

Fig 3.4 Principle of EDAX

To stimulate the emission of characteristic X-rays from a specimen, a high energy beam of charged particles such as electrons or a beam of X-rays, is focused with the sample being studied. At rest, an atom within the sample contains ground state (or unexcited) electrons in discrete energy levels or electron shells bound to the nucleus. The incident beam may excite an electron in an inner shell, ejecting it from the shell while creating an electron hole where the electron was. A position vacated by an ejected inner shell electron is eventually occupied by a higher energy electron from an outer shell and the difference in

energy between the higher energy shell and the lower energy shell may be released in the form of an X-ray. The amount of energy released by the transferring electron depends on which shell it is transferring from, as well as which shell it is transferring to. The number and energy of the X-rays emitted from a specimen can be measured by an energy dispersive spectrometer. As the energy of the X-ray is characteristic of the difference in energy between the two shells, and of the atomic structure of the element from which they were emitted, this allows the elemental composition of the specimen to be measured.

3.3.5 Atomic Force Microscopy (AFM)

Atomic force microscopy is arguably the most versatile and powerful microscopic technology for studying samples at nanoscale. It is versatile because an atomic force microscope can not only image in three-dimensional topography, but it also provides various types of surface measurements. It is powerful because an AFM can generate resolution with angstrom scale with minimum sample preparation.Atomic Force Microscope Agilent 5100 was used to record the AFM images.

An Atomic Force Microscope is simply an extremely small, sharp probe attached to a spring loaded cantilever that is moved over the surface of a sample. Light from a laser shining on the cantilever is detected by a photodiode and the signal interpreted by specialist electronics. The tip is normally made from a ceramic or semiconducting material but tips are now being made from carbon nanotubes.

In order to ‘read’ the sample, the tip can be dragged smoothly over the surface or repeatedly tapped on the surface. Dragging the tip on the surface is known as “Contact Mode” and tapping the surface is “Tapping Mode”. Another mode is also available, Non-Contact Mode. In non-contact mode the tip doesn’t actually touch the material surface but rather measures attractive forces between to sample and tip.

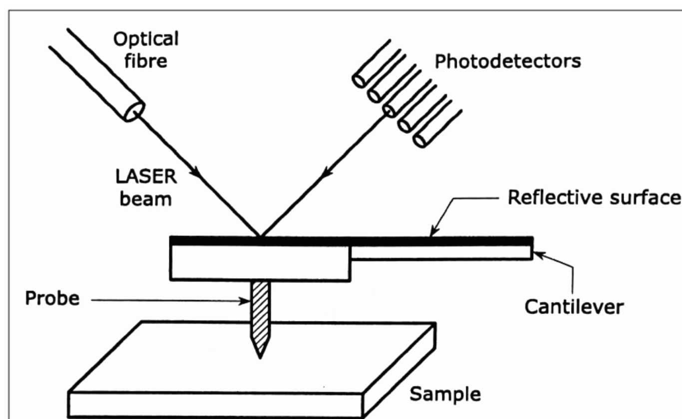

Fig 3.5 Block diagram of Atomic Force Microscope

AFM tips are normally shaped like a pyramid and manufactured using microlithographic techniques. The sharper the tip, the better will be the resolution of the final image. The problem with these tips is that they can become snagged in narrow valleys in the sample and be broken, damaged or simply remain stuck. Tips are now being made from cylindrical carbon nanotubes that are much stronger, but flexible.

3.3.6 Ultra-Violet-Diffuse Reflectance Spectroscopy (UV-DRS)

In the UV/Visible wavelength range upon interaction with a sample, four results are possible: the radiation is absorbed, transmitted, reflected or scattered. Typically UV/Vis spectrometers are equipped to measure the transmittance or absorbance of a transparent solid or homogenous solution. However, when equipped with the proper accessories, UV/Vis instruments can measure the reflected and scattered energy from a sample. Reflected radiation can be either specular or diffuse. An integrating sphere, when used in combination with the UV-Vis spectrometer, is a valuable tool for collecting and measuring specular and/or diffuse reflectance. In addition, an integrating sphere can be used to capture the scattered light from a sample. The integrating sphere is placed in the sample beam of the spectrometer and is used in place of the sample beam detector. The instrument detector, external to the sphere, detects the reference beam. The sphere can be used over the wavelength range of 250

nm to 1100 nm for either diffuse reflectance or diffuse transmittance. Alternatively, by placing a sample at the exit of the sphere, reflected light is collected and measured at the detector in diffuse reflectance mode. The sphere is easily installed in the standard sample compartment of the spectrometer making it easy to switch between normal transmittance and diffuse reflectance/transmittance modes. Liquid, powder and solid color samples can be determined easily.

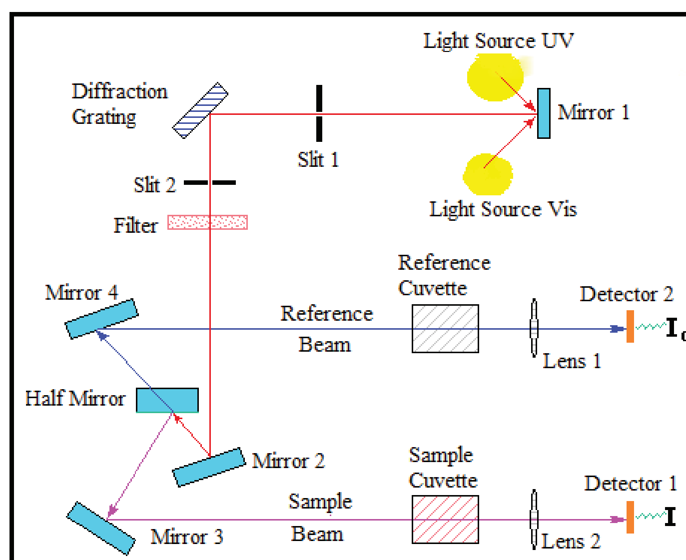

Fig 3.6 Schematic diagram of UV-Vis DRS Spectrophotometer.

The theory which makes possible to use DR spectra was proposed by Kubelka and Munk

$$\frac{K}{S} = \frac{(1 - R_\infty)^2}{2R_\infty} \equiv FR_\infty$$

Where F(R_∞) is usually termed the remission or Kubelka–Munk (K–M) function, K and S are the absorption and scattering coefficient of the sample, respectively. The bandgap can be obtained from the plots of $[F(R_\infty)h\upsilon]^{1/2}$ versus hυ, as the intercept of the extrapolated linear part of the plot at $[F(R_\infty)h\upsilon]^{1/2} = 0$, assuming that the absorption coefficient α is proportional to the Kubelka–Munk function F(R_∞).The UV-DRS spectra of the thin films were obtained

by Agilent CARY 500 UV-VIS-NIR spectrophotometer at wavelength range of 300–1100 nm.

3.3.7 Photoluminescence spectroscopy

Photoluminescence spectroscopy is a contactless, nondestructive method of probing the electronic structure of materials. Light is directed onto a sample, where it is absorbed and imparts excess energy into the material in a process called photo-excitation. One way this excess energy can be dissipated by the sample is through the emission of light, or luminescence. In the case of photo-excitation, this luminescence is called photoluminescence.

Photo-excitation causes electrons within a material to move into permissible excited states. When these electrons return to their equilibrium states, the excess energy is released and may include the emission of light (a radiative process) or may not (a nonradiative process). The energy of the emitted light (photoluminescence) relates to the difference in energy levels between the two electron states involved in the transition between the excited state and the equilibrium state. The quantity of the emitted light is related to the relative contribution of the radiative process.

The essential components of a spectrofluorometer are a light source, an excitation monochromator, a sample cell/cuvette, an emission monochromator and a detector. The light source sends out light at the excitation wavelength of an analyte in a sample. Before it reaches the sample, the light passes through the excitation monochromator, which transmits a wavelength specific to the excitation spectrum of the analyte while blocking other wavelengths. The light from the excitation monochromator passes through the sample contained in the sample cell/cuvette holder and excites the analyte. Following excitation, the analyte relaxes and emits light at an emission wavelength longer than the excitation wavelength. The emitted light passes through the emission monochromator positioned at a

right angle to the excitation light. The emission monochromator minimizes light scatter and screens the emission light before it reaches the detector. The detector measures the emitted light, displays the fluorescence value and produces the fluorescence signature of the analyte.

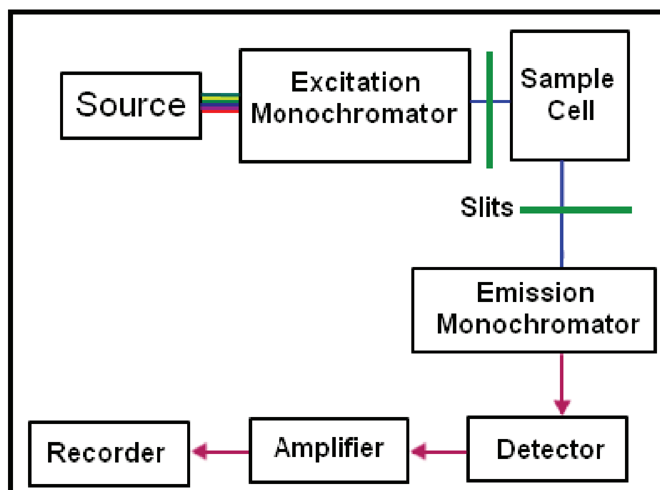

Fig 3.7 Schematic diagram of Fluorescence spectrophotometer.

The fluorescence value is proportional to the concentration level of the analyte in the sample. The fluorescence signature can be correlated to the concentration level of the analyte in the sample. The photoluminescence spectra of the films were recorded on SHIMADZU RF-6000 spectrofluorophotometer.

3.3.8 Vibrating sample magnetometer (VSM)

The basic operating principle of vibrating sample magnetometer (VSM) is based on Faraday's Law of Induction (i.e. changing magnetic flux will produce an electric field). The generated electric field can be measured and can tell us information about the changing magnetic field. A VSM is employed to measure the magnetic behavior of magnetic materials.

A VSM operates by first placing the sample to be studied in a constant magnetic field. If the sample is magnetic, the external magnetic field will magnetize the sample by aligning the individual magnetic spins or the magnetic domains, with the applied field. The stronger the external magnetic field, the larger the magnetization will be in the material. The magnetic

field around the sample will generate due to magnetic dipole moment of the sample, sometimes called the magnetic stray field. As the sample is vibrated (i.e. moved up and down), the magnetic stray field will be changed as a function of time and a set of pick-up coils will sense the same.

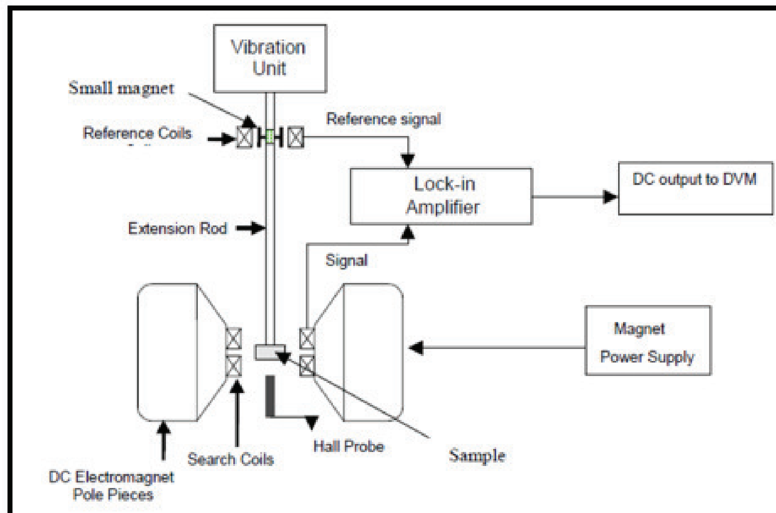

Fig 3.8 A schematic layout of the Vibrating Sample Magnetometer

According to Faraday's Law of induction the alternating magnetic field will cause an electric field in the pick-up coils. This current is directly proportional to the magnetization of the sample. The induction current is amplified by a trans impedance amplifier and lock-in amplifier. The assorted components are connected to computer interface. By means of controlling and monitoring software, the system can show the data on how much the sample is magnetized and how its magnetization depends.

The B-H hysteresis loop tracer is essentially two coils, one with a sample and the other which is empty for comparison. The insertion of a sample into the pickup coils causes a voltage proportional to the rate of change of the vector field to occur across the difference amplifier. After passing through an integrator, a voltage proportional to the intrinsic induction is passed to the Y-amp of the oscilloscope. This voltage combined with an X-voltage

representing the magnetising field generated from the solenoid without the sample results in the generation of a hysteresis loop on the oscilloscope. Calibration is through a balance and phase adjustment to establish a trace on the oscilloscope. They are done to make sure that the magnetising field is linear and that every vector corresponds to the applied field. Measurements for the magnetic properties can then be made.The coils have the ability to heat the sample such that temperature variance can be observed in the way that the material behaves when influenced by a magnetic field. A BH-looper can give the user a more improved visualisation compared to a VSM of the way a material behaves. The values plotted on the scope are only proportional to the absolute values, therefore display yields qualitative not quantitative information about a material magnetic properties.

3.3.9 Electrochemical Impedance Spectroscopy (EIS)

Electrochemical impedance spectroscopy (EIS) is a powerful tool to investigate electrochemical systems. The advantage of EIS is that it is generally non-destructive system. EIS is the most common method for measuring the equivalent series resistance (ESR) of electrochemical capacitors. It also allows creating methods to describe underlying reaction mechanisms. EIS is also used for the characterization of electrical properties of different materials, including conductors, semiconductors and even insulators (J.R. Macdonald, 2007).

Normally, EIS is conducted at the open-circuit voltage (OCV) by applying a small amplitude of alternative potential (5 ~ 10 mV) in a range of frequency (generally 0.01 to 100Hz). The resistance (Z) is defined as $Z = Z' + jZ''$, where Z' and Z'' are the real part and the imaginary part of impedance, respectively.

In general, EIS measures the dielectric properties of a medium as a function of frequency. In the case of an ideal resistor, the resistance can be calculated using Ohm's law in terms of the ratio between the voltage E and the current I, where $R = E/I$. However, in the real world there are different types of resistance for more complex systems, in which case we use

impedance. The electrochemical impedance is calculated by measuring the current through the cell when an AC potential is applied at different frequencies, f (Hz). Typically, the current response to a sinusoidal potential is also sinusoidal at the same frequency but with a phase shift. The change in potential E_t at time (t) is related to the maximum potential E_0 as a function of the radial frequency ω (radian/second), as follows:

$$E_t = E_0 \sin(\omega t), \text{ where } \omega = 2\pi f$$

On the other hand, the current at time t (I_t) is shifted in phase and is related to the maximum current (I_0) according to

$$I_t = I_0 \sin(\omega t + \phi), \text{ where } \phi \text{ is the phase shift}$$

Consequently, the impedance (Z) of the system is calculated as follows:

$$Z = E_t/I_t = E_0 \sin(\omega t)/ I_0 \sin(\omega t + \phi) = Z_0 \sin(\omega t)/\sin(\omega t + \phi), \text{ where } Z_0 = E_0/I_0$$

The impedance can also be expressed as a complex number for calculating the real part (Z_{re}) and imaginary part (Z_{im}) of the impedance at different frequencies, where

$$Z(\omega) = E/I = Z_0 \exp(j\phi) = Z_0 (\cos\phi + \text{i} \sin \text{j}\phi), \text{ where } j = \sqrt{-1}$$

As the majority of electrochemical cells do not have a uniform current, leading to the urgent need for EIS mathematical representation that can be fitted theoretically to a simulated model. Nyquist plot is the conventional mathematical data representation for resistance quantification. Typically, the imaginary part of impedance Z_{Im} (Z”) is plotted against the real part Z_{Re} (Z’) at different values of frequencies ω. In a standard Nyquist plot, the semicircle portion at higher frequencies corresponds to electron transfer limited process, Figure 3.9 shows the Nyquist Plot for an equivalent circuit with R_{ct} = 100 Ω, where the charge-transfer resistance can found by reading the real axis value at the high frequency intercept (A.J. Bard and L. R. Faulkner, 2001).

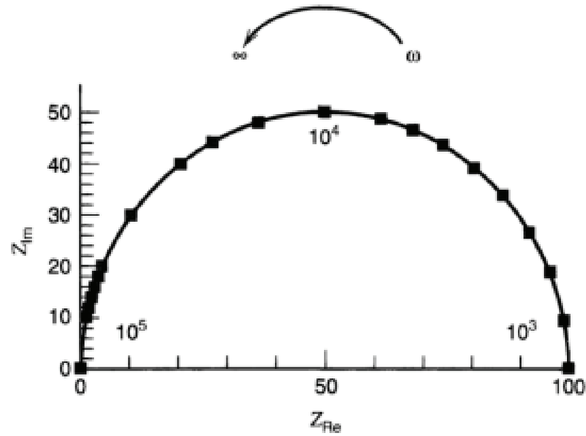

Fig. 3.9 Nyquist plot for an equivalent circuit with R_{ct} = 100 Ω

It is notable that a large semicircle observed from a Nyquist plot is an indicative of high charge-transfer resistance, contributing to the poor electrical conductivity of materials, whereas a more vertical the line is more closing to an ideal capacitor. In characterizing systems with capacitive behaviour, it is suggested that the frequency range can be divided into three regions: high-frequency region, medium frequency region and low frequency capacitive region (D.B. Williamsa& C.B. Carter 1996, L.R. Whitman et.al 2011). The high-frequency and medium frequency is divided by the knee frequency. The low-frequency region is characterized by a slope of -1 in Bode plot; ideal capacitive behaviour can be observed at the frequency f_0 at which phase-angle = -45°, and the reciprocal of f_0 is defined as characteristic response time (τ_0). Obviously, we can see that smaller the τ_0, faster the response would be and thus better pulse power performance. The quantitative data for these parameters can be obtained by fitting the impedance spectra using the electrical equivalent circuit. The most common equivalent circuit model for better quantification of the effects of different parameters is the simplified Randles equivalent circuit model, which consists of a solution resistance (R_s), a double layer capacitor (C_{dl}), a charge transfer resistance (R_{ct}), and Warburg impedance element (Z_W). In this model, the

double-layer capacitance is in parallel with the charge-transfer resistance, as shown in Figure 3.10.

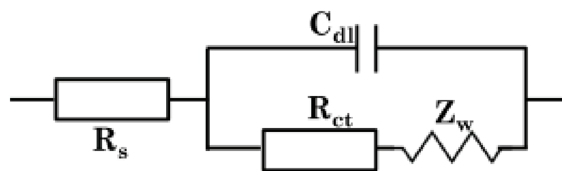

Fig. 3.10 Schematic diagram of the simplified Randles equivalent circuit.

The impedance of an electrochemical cell could be due to the solution resistance between the counter and reference electrodes or between the reference and working electrodes. There are many parameters that affect and contribute to the solution resistivity (R_s) and they generally include electrolyte ion type, electrolyte concentration, and deposition active surface area.

In addition, as ions diffuse in an electrolyte solution, they could be adsorbed onto the electrode surface forming a double layer. The existence of this electrical double layer at the interface would separate the ions from the charged electrode by an insulating space, forming a capacitor (C_{dl}). Many parameters, such as ionic concentration, electrode potential, and impurity adsorption, could affect the magnitude of the capacitor (M.E. Orazem & B. Tribollet 2008, J.S. Newman & K. E. Thomas-Alyea 2004).

Another type of resistance that exists in the electrochemical cell is the charge transfer resistance (R_{ct}), which occurs when the electrons enter the electrolyte solution and the metal ions start to diffuse into the electrolyte after their dissolution according to: $M \leftrightharpoons M_n^+ + ne^-$ This type of resistance is our main interest in order to characterize the as-prepared photo-anodes charge transfer process efficiency.

Finally, the Warburg impedance (Z_w) element represents the mass transfer resistance used in the equivalent circuit model. In contrast to electrolyte resistance (R_s) and double layer capacitance (C_{dl}), the Warburg impedance (Z_w) is a non-ideal circuit element as it changes with the frequency, ϖ. However, the identification of Z_w is difficult because it is always accompanied with the charge-transfer resistance and double-layer capacitance.

In the present thesis, a CHI660C electrochemical workstation was used to perform electrochemical impedance spectroscopy. The three electrode cell has been formed using Ag/AgCl (reference electrode), a platinum wire of diameter 0.5 mm (counter electrode) and the as-grown samples (Pure and Magnesium doped CuI NPs on glass substrates) as working electrodes. All the electrochemical characterization was carried out at room temperature (300 K) in 0.1 M sodium hydroxide aqueous solution (electrolyte). EIS measurements were carried out over the frequency range (10 mHz-100 kHz) with 5mV amplitude around the open circuit potential (OCP).

3.3.10 Computational details

The first principle calculation of zinc blende CuI (space group: *F43m*) structure is performed by solving Kohn – Sham equation using full potential linearized augmented plane wave (FP – LAPW) method which is a part of the DFT as implemented in Wien2k code (P. Blaha, 2001). The structural, electronic and linear optical properties of CuI structure is calculated using GGA exchange correlation potential proposed by Perdew – Burke – Emzerholf (PBE). Since this method underestimates the energy gap and fares poorly in locating *d* and *f* orbitals the present calculations are performed using modified Becke Johnson (mBJ) potential for obtaining more accurate results.

In this FP-LAPW method, there are no shape approximations to the charge density or potential. Space around the atoms in the unit cell is divided into two regions such as, (*i*) a spherical muffin-tin (MT) around the nuclei in which the radial solutions of the Schrödinger

equation and their energy derivatives are used as basic functions, (*ii*) the interstitial region between the muffin-tins, in which the basis set consists of plane waves (KE. Babu et.al, 2014). The cut-off energy which defines the separation between the core and valence states is set at −6.0 Ry. The atomic position and sphere radii used are (000) and 2.04 *a.u.* for Cu (1/4 1/4 1/4) and 2.43 *a.u*. for I, respectively. Augmented plane wave (APW) plus local valence orbitals are used with the wave functions, while the potentials and charge densities are expanded in terms of spherical harmonics inside the muffin-tin spheres. Well-converged solutions were obtained with $R_{MT} K_{max.} = 7.0$ (where R_{MT} is the smallest muffin-tin radii and K_{max} is the plane wave cut-off) and *k*-point sampling is checked. Self-consistent calculations are considered to converge when the total energy of the system is stable within 0.0001 Ry. The optoelectronic properties of the compound are calculated using a denser mesh of 1000 *k*-points in the irreducible Brillouinzone (IBZ). The DFT method has proven to be one of the most accurate methods for the computation of the electronic structure of solids (AH. Reshak 2011, 2013, 2014, GE. Davydyuk et.al 2013).